2013 IEEE/RSJ International Conference on
Intelligent Robots and Systems (IROS)
November 3-7, 2013. Tokyo, Japan

Controlling Aerial Maneuvering of a Miniature Jumping Robot Using Its Tail

Jianguo Zhao, Tianyu Zhao, Ning Xi, Fernando J. Cintrón, Matt W. Mutka, and Li Xiao

Abstract— **In this paper, we present the design and experimentation of a miniature robot that can jump, run, and perform aerial maneuvering. Specifically, this robot can use wheeled locomotion to run on the ground. Encountering an obstacle, it can jump up to overcome the obstacle. After leaping into the air, the robot can control its body angle using its tail for aerial maneuvering. To the best of our knowledge, this is the first miniature (maximum size 6.5 centimeters) and lightweight (28.0 grams) robot that having all the three capabilities. Furthermore, this robot is equipped with on-board energy, sensing, control, and wireless communication capabilities, which enables the tetherless operation. It can be potentially employed for mobile sensor networks in environments with obstacles.**

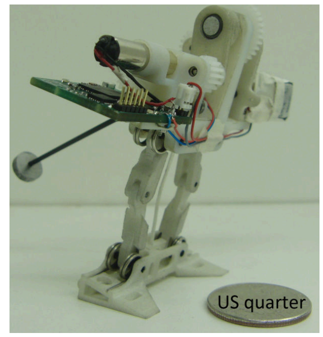

Fig. 1. The robot prototype.

I. INTRODUCTION

In nature, many animals use multiple locomotion methods to travel in environments [1], which can minimize the energy consumption in different situations. For example, a frog can rapidly jump to seize small insects or escape predators, but they can also walk slowly in other situations. The various locomotion abilities found in animals can inspire novel robot designs with multi-modal locomotion.

As the deployment of robots in natural environments becomes more widespread, it is necessary to design multi-modal locomotion robots. Consider the scenario of using many miniature robots to monitor an environment with obstacles. The energy efficient way is to use wheeled locomotion when no obstacle exists. Encountering a large obstacle, the robot can jump over it. Moreover, to protect the robot from damage during the landing, it is desirable that the robot can perform aerial maneuvering to control its body angle to land on the ground with a safe posture. The objective of the study in this paper aims to design a robot that can accomplish the above multi-modal locomotion.

Jumping locomotion has advantages over other methods such as wheeled, legged, or flying locomotion. In fact, it enables the robot to overcome large obstacles with a relative small energy consumption. Compared with the wheeled or legged locomotion, the robot can overcome obstacles with sizes more than 13 times the maximum robot size [2]. Compared with the flying locomotion, the energy consumption for jumping is smaller since the robot does not need to stay aloft. In addition, jumping can enhance the wireless communication range for sensors [3].

This work is supported by the National Science Foundation under Grant NO. CNS-0721441

Jianguo Zhao and Ning Xi are with Department of Electrical and Computer Engineering, Michigan State University, East Lansing, MI, 48824, USA. zhaojia1@msu.edu, xin@egr.msu.edu

Tianyu Zhao is with Department of Mechanical Engineering, Michigan State University, East Lansing, MI, 48824, USA. zhaotian@msu.edu

Fernando J. Cintrón, Matt W. Mutka and Li Xiao are with Department of Computer Science and Engineering, Michigan State University, East Lansing, MI, 48824, USA. {cintrong, mutka, lxiao}@cse.msu.edu

With the merits of jumping locomotion, many jumping robots have been developed in recent years, and a detailed review can be found in [2]. Representative jumping robots include the frogbot [4], the EPFL jumper V3 [5], the Grillo [6], the Jollbot [7], the flea [8], and our three generations of jumping robot [9], [10], [11].

Although jumping can be used as a locomotion method, the energy consumption is large if the robot jumps to travel on flat ground [12]. In this case, wheels are the most energy efficient method. Therefore, we should combine jumping and wheeled locomotion in a single robot.

Researchers have studied multi-modal wheeled and jumping robots as well. Examples include the scout robot [13], the mini-whegs [14], the rescue robot [15], the stair climbing robot [16], and the recent sand flea from Boston Dynamics [17]. However, these robots are heavy ones, with weights ranging from 200 grams for the mini-wheg to 5000 grams for the sand flea. In contrast, our robot is designed to be less than 30 grams. With a light weight, the energy consumption for jumping to the same height is small; moreover, the robot is less susceptible to the damage from the landing impact.

Besides the multi-modal wheeled and jumping locomotion, the aerial maneuvering ability can make the robot land on the ground with a safe posture to reduce the damage at landing. Furthermore, if the robot is employed for mobile sensor nodes in wireless sensor network, it can send data to other sensors in a specific direction.

Many small animals swing their tails to control the body orientation such as geckos [18] and lizards [19], [20]. Recently, researchers built robot prototypes to investigate the merits of tail assisted robots. Chang-Siu *et al.* [21] added

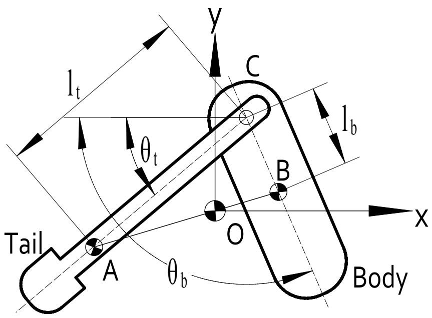

Fig. 2. The schematic of the robot in the air.

a tail to a wheeled robot to control the robot's pitch angle during free fall. Johnson *et al.* [22] also appended a tail to a legged robot to control the robot's pitch angle for safe landing from some height. Demir *et al.* [23] found that an appendage added to a quadrotor could enhance the flight stabilization. Briggs *et al.* [24] added a tail to a cheetah robot for rapid dynamic running and disturbance rejection. Kohut *et al.* [25] studied the dynamic turning of a miniature legged robot using a tail on the ground.

In this paper, we aim to realize the objective of efficient traveling in environments with obstacles. Towards this goal, we design and develop a miniature lightweight multi-modal robot that has three capabilities: running using wheeled locomotion on the ground, jumping to overcome large obstacles, and aerial maneuvering to control its body angle using an active tail. Although there exist robots having one or two abilities, to the best of our knowledge, this is the first robot having all the three. Moreover, the robot has a light weight of 28.0 grams and a maximum size of 6.5 centimeters.

The rest of this paper is organized as follows. In section II, the dynamics model for mid-air maneuvering is presented. In section III, the design for both the mechanical and electrical part is elaborated. After that, experimental results for the robot's various functions are presented in section IV.

II. Dynamics Modeling For Aerial Maneuvering

To perform aerial maneuvering in the mid-air, we need at least two control inputs to control the three rotational degree-of-freedom [20]. As our first step, however, we consider a simplified case when only one control input is applied. Specifically, we control the robot body's pitch angle using a tail actuated by a DC motor.

We need the dynamics model for the robot in the mid-air to perform aerial maneuvering. In this paper, we derive the dynamics equation using the Euler-Lagrange method. Moreover, we obtain a general system dynamics with the actuator's angle as the state variable, which will guide the optimal tail design in the next section.

The schematic of the robot in the mid-air is shown in Fig. 2. The robot consists of a body part and a tail part, which are connected by an actuated revolute joint at point C. Suppose the center of mass for the tail, body, and whole robot be at point A, B, and O, respectively. We use the parameters listed in Table I in the following discussions.

TABLE I

List of parameters for dynamics modeling

m_b	body mass
m_t	tail mass
l_b	length of link BC
l_t	length of link AC
θ_b	body angle with respect to the horizontal line
θ_t	tail angle with respect to the horizontal line
I_b	moment of inertial for the body
I_t	moment of inertial for the tail

For the system in Fig. 2, a frame $OXYZ$ is attached to the robot with X axis along the horizontal direction, Y axis along the vertical direction, and Z axis (not shown in the figure) determined by the right hand rule. In such a frame, we obtain the coordinates $\vec{A} \in \mathbb{R}^3$ and $\vec{B} \in \mathbb{R}^3$ for point A and point B, respectively, to derive the dynamics equation.

To apply the Euler-Lagrange method, we first derive the Lagrangian for the system. With the coordinate system $OXYZ$, the robot's translational motion is decoupled from the rotational motion [26]. Since the translational motion is a simple projectile motion [2], we only consider the rotational motion for aerial maneuvering. Without the translational motion, the robot's potential energy is zero. Therefore, the Lagrangian is just the system's kinetic energy:

$$\begin{aligned}\mathscr{L} &= \frac{1}{2}I_t\dot{\theta}_t^2 + \frac{1}{2}m_t||\dot{\vec{A}}||_2^2 + \frac{1}{2}I_b\dot{\theta}_b^2 + \frac{1}{2}m_b||\dot{\vec{B}}||_2^2 \\ &= \frac{1}{2}[I_t\dot{\theta}_t^2 + I_b\dot{\theta}_b^2 + \frac{m_t m_b}{m_t+m_b}(l_t^2\dot{\theta}_t^2 + l_b^2\dot{\theta}_b^2 - 2l_t l_b\dot{\theta}_t\dot{\theta}_b\cos\theta_m)]\end{aligned}$$

where $\theta_m = \theta_b - \theta_t$ is the actuator's rotation angle. Neglecting the air resistance and applying the Euler-Lagrange method, we can obtain dynamics equation for the system as:

$$M\ddot{\theta}_t - L\cos\theta_m\ddot{\theta}_b + L\sin\theta_m\dot{\theta}_b^2 = \tau \quad (1)$$

$$N\ddot{\theta}_b - L\cos\theta_m\ddot{\theta}_t - L\sin\theta_m\dot{\theta}_t^2 = -\tau \quad (2)$$

where

$$M = I_t + \frac{m_t m_b l_t^2}{m_t+m_b}, \quad N = I_b + \frac{m_t m_b l_b^2}{m_t+m_b}, \quad L = \frac{m_t m_b l_t l_b}{m_t+m_b}$$

Note that we only have one τ for external forces because of the single actuator.

For the system described by Eqs. (1) and (2), if both θ_t and θ_b should be controlled to desired values, then the system is underactuated since there is only one input τ. In this paper, however, we only care about the robot body angle θ_b. To control θ_b, (1) and (2) should be transformed into a single equation to eliminate θ_t, but this is impossible due to the coupling between θ_t and θ_b. Nevertheless, we can transform Eqs. (1) and (2) to a new equation with only θ_m as the variable as shown in the following steps.

First, we solve $\ddot{\theta}_t$ and $\ddot{\theta}_b$ from Eqs. (1) and (2):

$$\ddot{\theta}_t = \frac{SL\dot{\theta}_t^2\cos\theta_m - SN\dot{\theta}_b^2 + R\tau}{T} \quad (3)$$

$$\ddot{\theta}_b = \frac{SM\dot{\theta}_t^2 - SL\dot{\theta}_b^2\cos\theta_m - Q\tau}{T} \quad (4)$$

where $Q = M - L\cos\theta_m$, $R = N - L\cos\theta_m$, $S = L\sin\theta_m$, $T = MN - L^2\cos^2\theta_m$. Since $T = MN - L^2\cos^2\theta_m \geq MN - L^2 > 0$, there is no singularity for using T as the denominator in Eqs. (3) and (4). From $(4)-(3)$ and $\ddot{\theta}_m = \ddot{\theta}_b - \ddot{\theta}_t$, we have:

$$\ddot{\theta}_m = \frac{SQ\dot{\theta}_t^2 + SR\dot{\theta}_b^2}{T} - \frac{Q+R}{T}\tau \tag{5}$$

Second, we utilize the conservation of angular momentum to eliminate both $\dot{\theta}_t$ and $\dot{\theta}_b$ in Eq. (5) by expressing them as a function of $\dot{\theta}_m$. In fact, the angular momentum for the total system can be obtained as: $H_0 = (M - L\cos\theta_m)\dot{\theta}_t + (N - L\cos\theta_m)\dot{\theta}_b$. Assume a zero angular momentum, i.e., $H_0 = 0$. Since $\dot{\theta}_m = \dot{\theta}_b - \dot{\theta}_t$, we can solve for $\dot{\theta}_t$ and $\dot{\theta}_b$ as follows:

$$\dot{\theta}_t = \frac{-R\dot{\theta}_m}{Q+R} \tag{6}$$

$$\dot{\theta}_b = \frac{Q\dot{\theta}_m}{Q+R} \tag{7}$$

Finally, plugging Eqs. (6) and (7) into (5), we can obtain:

$$\ddot{\theta}_m = \frac{QRS\dot{\theta}_m^2}{T(Q+R)} - \frac{Q+R}{T}\tau \tag{8}$$

If the revolute joint is driven by a DC motor, then the torque τ, under a constant voltage supply, is related to its angular speed $\dot{\theta}_m$ by: $\tau = \tau_s(1 - \dot{\theta}_m/\omega_n)$, where τ_s is the motor's stall torque and ω_n is its no-load angular speed. With this equation, Eq. (8) becomes:

$$\ddot{\theta}_m = \frac{QRS\dot{\theta}_m^2}{T(Q+R)} - \frac{Q+R}{T}\tau_s\left(1 - \frac{\dot{\theta}_m}{\omega_n}\right) \tag{9}$$

From the equation, we can solve for $\theta_m(t)$ for a DC motor with a constant voltage supply. With $\theta_m(t)$, we can finally obtain body angle's trajectory from Eq. (7):

$$\theta_b(t) = \int_0^t \frac{Q\dot{\theta}_m}{Q+R}dt + \theta_b(0) \tag{10}$$

where $\theta_b(0)$ is the initial body angle. Therefore, we can obtain the time to reach the desired angle θ_b^* from any initial angle $\theta_b(0)$.

Libby and Chang-Siu *et al.* obtained the same dynamics in Eqs. (1) and (2) using the Newtonian mechanics [19], [21]. However, they directly utilized the equations to perform the optimal tail design under a constant maximum torque τ. In reality, the maximum torque cannot be applied due to the motor's dynamics. Therefore, Eqs. (9) and (10) provide a more precise model for the optimal design in the next section.

III. Robot Design And Implementation

In terms of functions, we divide the robot into four parts: the jumping part, the tail part, the running part, and the embedded control system part. The solid model of the robot is shown in Fig. 3(a). Since the jumping part comes from our previous design [2], [27], we omit the details here. In this section, we discuss the other three parts in detail.

A. Tail Part Design

Tail part design ensures successful aerial maneuvering. The design should be able to rapidly change the body's orientation since the jumping process lasts for a short time. Therefore, we choose to obtain an optimal design that maximizes the change of θ_b for a given time.

We perform the optimal design based on the dynamics equations (9) and (10). The optimal design is carried out in four steps: identifying optimization variables, formulating the objective function, obtaining the constraints, and solving the constraint optimization problem.

We first identify the optimization variables. To simplify the design, we choose the tail motor empirically (GH6123S from Gizmoszone). We also assume another gear train with a speed reduction ratio r to adjust the relationship between the speed and the torque from the motor. The tail is implemented by attaching a steel block at the end of a carbon fiber rod. Since the rod has a negligible mass compared with the block, the tail's moment of inertial I_t can be approximated as $I_t = m_t l_t^2$. Since m_b, l_b, and I_b are known based on our previous jumping robot [2], the remaining unknown parameters m_t, l_t, and r are the optimization variables.

The objective function for the optimization problem is θ_b. We choose the design that will maximize the change of θ_b under a small fixed time period (0.1 s). In this case, θ_b can be expressed as a function of m_t, l_t, and r using Eqs. (9) and (10). Denote this function as $\theta_b = f(m_t, l_t, r)$.

The optimization constraints are derived as follows. Since a large tail weight will decrease the jumping performance and increase the landing impact, we let $m_t \leq 0.15m_b$. On the other hand, since m_t cannot be too small to perform effective aerial maneuvering, we constrain $m_t \geq 0.05m_b$. With similar practical reasons, we let $0.75L_b \leq l_t \leq 1.5L_b$ and $0.1 \leq r \leq 10$ with $L_b = 6.5$ cm being the body length.

Based on previous discussions, the optimal design problem is formulated as:

$$\begin{array}{rl} \max & \theta_b(0.1) = f(m_t, l_t, r) \\ \text{subject to} & 0.05m_b \leq m_t \leq 0.15m_b, 0.75L_b \leq l_t \leq 1.5L_b \\ & 0.1 \leq r \leq 10 \end{array}$$

The problem is solved using the Optimization Toolbox in Matlab. The optimal result is $m_t = 1.35$ gram, $l_t = 6.56$ cm, and $r = 2.17$. With the optimal parameters, θ_b can change 80 degrees in 0.1 s. To accommodate the available off-the-shelf gears, we let $r = 2$. In this case, the change of θ_b only decreases about 0.1%.

The solid model for the tail part is shown in Fig. 3(b). The motor gear has eight teeth, while the tail gear has sixteen teeth. The motor gear is directly actuated by the tail motor, and the tail is inserted to a hole in the tail gear. Two teeth of the tail gear are removed to avoid the interference between the tail and the robot body at the limit positions. This is also useful for the running part that will be discussed in the next sub section.

The tail can also be utilized for self-righting. Since the robot has a rectangular shape with two surfaces larger than

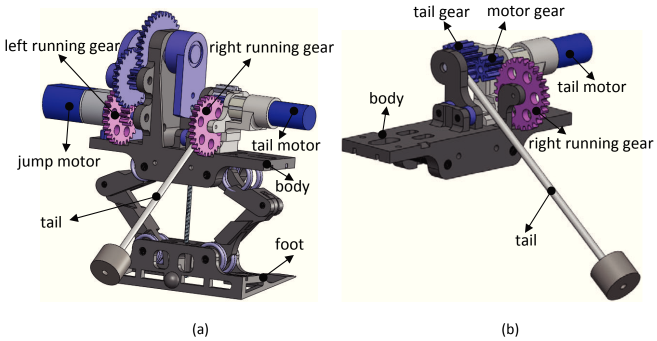

Fig. 3. Robot Model: (a) the solid model for the whole robot and (b) the solid model for the tail part.

the other four, it will contact the ground with one of the two large surfaces after landing on the ground. No matter which large surface contacts the ground, the robot can stand up for the next jump by using the tail to push the ground.

B. Running Part Design

As shown in Fig. 3(a), the running part employs two running gears for differential drive. As mentioned in the tail design, the robot will land on the ground with one of the two large surfaces. If the robot lands on the ground with the surface having the two running gears, it can perform the wheeled locomotion. If the robot lands with the other large surface, the tail can rapidly rotate to turn the robot around to the posture for running.

No extra actuation is required for the running part. The left running gear is part of the jumping part actuated by the jump motor as shown in Fig. 3(a), while the right running gear is actuated by the tail motor as shown in Fig. 3(b). The tail gear in Fig. 3(b) has two teeth removed. Once the tail reaches the limit position when the tail contacts left side of the body, further rotation of the motor gear cannot actuate the tail. In this case, the right running gear can perform the wheeled locomotion.

The turning motion is realized by actuating one running gear while keeping the other one still. Therefore, the robot can turn in both counterclockwise and clockwise directions.

C. Embedded Control System Design

A miniature embedded system controls the robot's motion. The system architecture is shown in Fig. 4. It is implemented

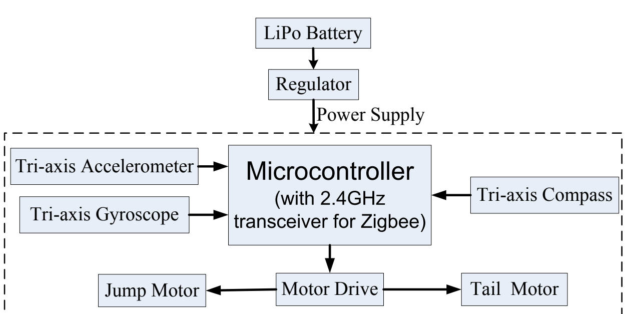

Fig. 4. Embedded control system architecture.

Fig. 5. Jumping experiment without actuating the tail: the robot is labeled with a circle and an arrow on the circle indicates the body's pitch angle.

by a printed circuit board with a dimension of $22.8mm \times 24.8mm$ and a mass of 3 g. The whole system has four parts: the central processing unit, the sensing unit, the actuation unit, and the power supply unit.

A microcontroller (ATmega128RFA1 from Atmel) serves as the central processing unit, which has an integrated 2.4GHz Zigbee transceiver. It enables the two-way data transmission between a computer and the robot. Moreover, with many robots, they are able to communicate with each other to form a mobile sensor network.

The sensing elements contains a tri-axis accelerometer, a tri-axis gyroscope, and a tri-axis magnetic compass. We use a single chip for the former two sensors (MPU-6050 from Invensense), while the compass is another chip (HMC5883L from Honeywell). The accelerometer can detect the free fall, while the gyroscope can feedback the body's angle and angular velocity to the microcontroller.

The actuation unit is a dual H-Bridge motor driver with pulse width modulation ability (MC34933 from Freescale) to control both the jump motor and tail motor. A FullRiver 50mAh LiPo battery—after being regulated to 3.3 V—powers the whole robotic system.

IV. Experimental Results

With the robot design presented in the previous section, we fabricated and assembled the robot prototype as shown in Fig. 1. We performed various experiments to test the individual functions of the robot.

A. Tail Assisted Jumping

We first tested the closed-loop orientation control using a PD controller when the robot underwent a free fall motion to tune the control parameters K_p and K_d. The detailed experimental results could be found in the accompanied video submission. After many experiments, we fixed the parameters as $K_p = 20$ and $K_d = 0.8$.

Based on the control parameters obtained from the free fall experiment, we then performed the tail assisted jumping—controlling the orientation once the robot jumped into the air. For comparison, we also carried out the jumping experiment without actuating the tail. Note that we had carefully adjusted the weight distribution of the robot to make it only have the desired planar motion in mid-air; however, we could not eliminate the rotation in other axes completely due to various disturbances such as the air resistance.

The experiment was setup as follows. We placed the robot on the ground and let it jump onto a desk with a height of

Fig. 6. Jumping experiment with tail actuated: the robot is labeled with a circle and an arrow on the circle indicates the body's pitch angle.

60 cm. To minimize the robot's slippage during take-off, we increased the coefficient of friction by placing the robot on a fine-grained sand paper. Moreover, we rotated the tail onto top of the body before the jumping to minimize the initial angular momentum.

During the experiment, a video was recorded by a Casio Exilim EX-FH25 high-speed camera with a frame rate 240 frames/s. Meanwhile, the body pitch angles were also recorded by the embedded control system. After landing, the robot sent the recorded data wirelessly to the computer.

Fig. 5 shows the result of jumping without actuating the tail. It has five frames extracted from the jumping video with the time showing at the left lower corner. From the figure, the angle does not change much and the robot lands on the desk with an unsafe posture (the landing posture is shown in the accompanied video submission). The body pitch angle is plotted by the dash-dotted line in Fig. 7. The initial angle is 100° and the angle changes to 90° after about 0.17 s. If there is no initial angular momentum, the angle should keep constant. The reason for this small change is that the tail can rotate slightly even it is not actuated due to the backlash between the tail gear and the motor gear.

The experiment with tail actuated was conducted as follows. The accelerometer first obtained the initial body angle. After the robot jumped up, the accelerometer detected the free fall and activated the PD controller. The gyroscope provided both the angular velocity and the angle for feedback, with the angle obtained by integrating the angular velocity. Based on these two feedback signals and the desired body pitch angle, the controller computed a velocity command for the tail motor.

Fig. 6 shows the results when the tail is actuated. The desired body pitch angle is set to 30° following the definition given in Fig. 2 (the angle is shown in the last picture of Fig. 6). After the robot leaps into the air, the tail starts to rotate and the body pitch angle approaches the desired value. Finally, the robot lands on the desk with a safe posture. The solid black line in Fig. 7 shows the body angle with respect to time. From the plot, the robot gradually reaches the desired angle but an overshoot occurs. The overshoot suggests the controller has a large settling time. But we cannot reduce the settling time by increasing the gain value since the largest body's angular velocity is very close to the gyroscope's measurement range ($\pm 500^\circ/s$). Note that although we can choose the measurement range as large as $\pm 2000^\circ/s$, the angle measurement is not accurate for control due to the drifting error for gyroscopes.

The ideal initial pitch angle for both experiments should be 105°—180° minus the robot's take-off angle 75°; however, the take-off angle may be slightly different (within $\pm 5^\circ$) for different jumps due to the implementation of the jumping mechanism.

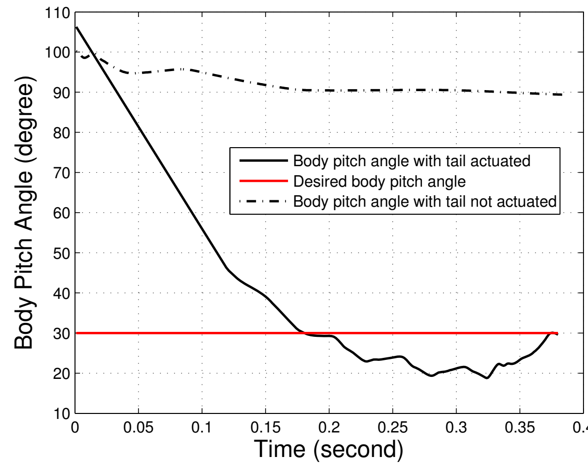

Fig. 7. Body pitch angle with respect to time during jumping.

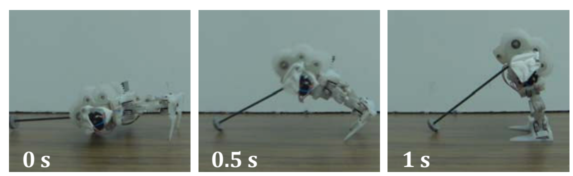

Fig. 8. Tail assisted self-righting experiment.

B. Tail Assisted Self-righting

As mentioned in the tail design, when the robot lands on the ground, the tail can have the robot stand up for the next jump. We also performed experiments for self-righting using the tail.

The experimental result for tail assisted self-righting from the left side is shown in Fig. 8, where three frames from a self-righting video are extracted. From the figure, the self-righting process is successfully achieved by rotating the tail. Additional experiments showing self-righting from the right side can be found in the video submission. In addition to the self-righting ability, the robot can also lay down for wheeled locomotion from a jumping posture by rapidly swinging the tail.

C. Running and Turning

Experiments were also conducted to test the running and turning performances. In the first experiment, the robot was

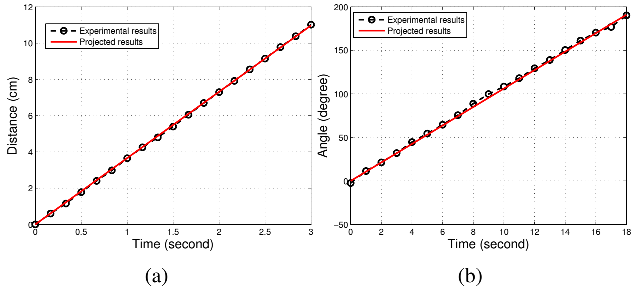

Fig. 9. Running and turning experiments: (a) running experimental results and (b) turning experimental results.

placed on a desk and beside a ruler to test the wheeled locomotion performance. We obtained the robot's position in the horizontal direction from the video every $1/6$ second. The positions with respect to time are plotted in Fig. 9(a) with a black dash line and the experimental data represented by small circles. By a linear regression of the experimental data, we obtain a red solid line shown in Fig. 9(a) with a slope 3.66 cm/s, which is the average running speed for the robot. The details for running are shown in the video submission.

To obtain the robot's turning performance, we placed it on the desk with a black line as a reference. After the robot started turning, we obtained the angle between the reference line and the robot every one second from the video. The angles with respect to time for 18 s are shown in Fig. 9(b) with the same style in Fig. 9(a). From the figure, we see the robot turns at an average angular velocity of $10.61°/s$, which is obtained by linear regression as well. The details for turning can also be found in the video submission.

V. Conclusions

We present a multi-modal running and jumping robot with aerial maneuvering ability in this paper. The robot uses wheeled locomotion to travel when no obstacle exists. Once there is an obstacle, the robot can jump over it. Moreover, the robot can control its pitch angle in the mid-air using an active tail. This way, it can control the landing posture to protect it from damage. Experimental results demonstrate all the functions of the proposed robot. The robot can perform energy efficient locomotion in environments with obstacles, which has many applications such as mobile sensor networks, military surveillance, and environmental monitoring.

References

[1] R. M. Alexander, *Principles of Animal Locomotion*. Princeton University Press, 2003.

[2] J. Zhao, J. Xu, B. Gao, N. Xi, F. J. Cintron, M. W. Mutka, and L. Xiao, "MSU jumper: A single-motor-actuated miniature steerable jumping robot," *IEEE Trans. on Robotics*, vol. 29, no. 3, pp. 602–614, 2013.

[3] F. Cintrón, K. Pongaliur, M. W. Mutka, L. Xiao, J. Zhao, and N. Xi, "Leveraging height in a jumping sensor network to extend network coverage," *IEEE Trans. on Wireless Communications*, vol. 11, no. 5, pp. 1840–1849, 2012.

[4] J. Burdick and P. Fiorini, "Minimalist jumping robots for celestial exploration," *Int. J. Robot. Res.*, vol. 22, no. 7, pp. 653–674, 2003.

[5] M. Kovac, M. Schlegel, J. Zufferey, and D. Floreano, "Steerable miniature jumping robot," *Auton. Robots*, vol. 28, no. 3, pp. 295–306, 2010.

[6] F. Li, W. Liu, X. Fu, G. Bonsignori, U. Scarfogliero, C. Stefanini, and P. Dario, "Jumping like an insect: Design and dynamic optimization of a jumping mini robot based on bio-mimetic inspiration," *Mechatronics*, vol. 22, no. 2, pp. 167–176, 2012.

[7] R. Armour, K. Paskins, A. Bowyer, J. Vincent, and W. Megill, "Jumping robots: a biomimetic solution to locomotion across rough terrain," *Bioinsp. Biomim.*, vol. 2, no. 3, pp. 65–82, 2007.

[8] M. Noh, S.-W. Kim, S. An, J.-S. Koh, and K.-J. Cho, "Flea-inspired catapult mechanism for miniature jumping robots," *IEEE Trans. Robotics*, vol. 28, no. 5, pp. 1007–1018, 2012.

[9] J. Zhao, R. Yang, N. Xi, B. Gao, X. Fan, M. W. Mutka, and L. Xiao, "Development of a self-stabilization miniature jumping robot," in *Proc. IEEE/RSJ Int. Conf. Intell. Robots Syst.*, St. Louis, MO, USA, 2009, pp. 2217–2222.

[10] J. Zhao, N. Xi, B. Gao, M. W. Mutka, and L. Xiao, "Design and testing of a controllable miniature jumping robot," in *Proc. IEEE/RSJ Int. Conf. Intell. Robots Syst.*, Taipei, Taiwan, 2010, pp. 3346–3351.

[11] ——, "Development of a controllable and continuous jumping robot," in *Proc. IEEE Int. Conf. Robot. Autom.*, Shanghai, China, 2011, pp. 4614–4619.

[12] Y. Pei, F. Cintrón, M. Mutka, J. Zhao, and N. Xi, "Hopping sensor relocation in rugged terrains," in *Proc. IEEE/RSJ Int. Conf. Intell. Robots Syst.*, St. Louis, MO, USA, 2009, pp. 3856–3861.

[13] S. Stoeter and N. Papanikolopoulos, "Autonomous stair-climbing with miniature jumping robots," *IEEE Trans. Systems, Man, and Cybernet-icsłPart B*, vol. 35, no. 2, pp. 313–325, 2005.

[14] B. G. A. Lambrecht, A. D. Horchler, and R. D. Quinn, "A small, insect inspired robot that runs and jumps," in *Proc. IEEE Int. Conf. Robot. Autom.*, Barcelona, Spain, 2005, pp. 1240–1245.

[15] H. Tsukagoshi, M. Sasaki, A. Kitagawa, and T. Tanaka, "Design of a higher jumping rescue robot with the optimized pneumatic drive," in *Proc. IEEE Int. Conf. Robot. Autom.*, Barcelona, Spain, 2005, pp. 1276–1283.

[16] K. Kikuchi, K. Sakaguchi, T. Sudo, N. Bushida, Y. Chiba, and Y. Asai, "A study on a wheel-based stair-climbing robot with a hopping mechanism," *Mechanical Systems and Signal Processing*, vol. 22, no. 6, pp. 1316–1326, 2008.

[17] E. Ackerman, "Boston dynamics sand flea robot demonstrates astonishing jumping skills," IEEE Spectrum Robotics Blog, 2012.

[18] A. Jusufi, D. Goldman, S. Revzen, and R. Full, "Active tails enhance arboreal acrobatics in geckos," *Proceedings of the National Academy of Sciences*, vol. 105, no. 11, pp. 4215–4219, 2008.

[19] T. Libby, T. Moore, E. Chang-Siu, D. Li, D. Cohen, A. Jusufi, and R. Full, "Tail-assisted pitch control in lizards, robots and dinosaurs," *Nature*, vol. 481, no. 7380, pp. 181–184, 2012.

[20] A. Jusufi, D. Kawano, T. Libby, and R. Full, "Righting and turning in mid-air using appendage inertia: reptile tails, analytical models and bio-inspired robots," *Bioinsp. Biomim.*, vol. 5, no. 4, p. 045001, 2010.

[21] E. Chang-Siu, T. Libby, M. Tomizuka, and R. J. Full, "A lizard-inspired active tail enables rapid maneuvers and dynamic stabilization in a terrestrial robot," in *Proc. IEEE/RSJ Int. Conf. Intell. Robots Syst.*, San Francisco, CA, USA, 2011, pp. 1887–1894.

[22] A. Johnson, T. Libby, E. Chang-Siu, M. Tomizuka, R. Full, and D. Koditschek, "Tail assisted dynamic self righting," in *Proceedings of the International Conference on Climbing and Walking Robots*, Baltimore, Maryland, USA, 2012, pp. 611–620.

[23] A. Demir, M. M. Ankarali, J. P. Dyhr, K. A. Morgansen, T. L. Daniel, and N. J. Cowan, "Inertial redirection of thrust forces for flight stabilization," in *Proceedings of the International Conference on Climbing and Walking Robots*, Baltimore, Maryland, USA, 2012, pp. 239–245.

[24] R. Briggs, J. Lee, M. Haberland, and S. Kim, "Tails in biomimetic design: Analysis, simulation, and experiment," in *Proc. IEEE/RSJ Int. Conf. Intell. Robots Syst.*, 2012, pp. 1473–1480.

[25] N. Kohut, A. Pullin, D. Haldane, D. Zarrouk, and R. Fearing, "Precise dynamic turning of a 10 cm legged robot on a low friction surface using a tail," in *Proc. IEEE Int. Conf. Robot. Autom.*, Karlsruhe, Germany, 2013, p. to appear.

[26] Z. Li and R. Montgomery, "Dynamics and optimal control of a legged robot in flight phase," in *Proc. IEEE Int. Conf. Robot. Autom.*, Cincinnati, OH, USA, 1990, pp. 1816–1821.

[27] J. Zhao, N. Xi, F. J. Cintron, M. W. Mutka, and L. Xiao, "A single motor actuated miniature steerable jumping robot," in *Proc. IEEE/RSJ Int. Conf. Intell. Robots Syst.*, Algarve, Portugal, 2012, pp. 4274–4275.